Exchange bias and nanoparticle magnetic stability in Co-CoO composites

J. A. De Toro, J. P. Andrés, J. A. González, P. Muñiz, T. Muñoz, P. S. Normile, and J. M. Riveiro
Departamento de Física Aplicada, Universidad de Castilla-La Mancha, 13071 Ciudad Real, Spain
(Received 11 November 2005; revised manuscript received 20 January 2006; published 30 March 2006)

A series of $Co_x(CoO)_{1-x}$ thin films have been synthesized by sputtering Co in an oxygen atmosphere using different rf sputtering powers as a means to vary the concentration x. The highest exchange-bias field ($H_E \approx 2.7$ kOe at $T=90$ K) was measured in a sample with an estimated metallic Co fraction of $x=0.53$. In this sample, and in those with lower Co concentrations, the temperature dependence of the magnetization shows a pronounced dip, both in zero-field- and field-cooled curves, at temperatures close to the Néel temperature of bulk CoO. This feature, which disappears with moderate annealing, is associated to the destabilization of small isolated Co nanoparticles when the exchange coupling with the CoO matrix vanishes above its Néel temperature. A simple structural model is proposed to account for the presented magnetization. X-ray diffraction and electrical resistivity results are also presented, which support the studies of magnetic properties.

DOI: 10.1103/PhysRevB.73.094449 PACS number(s): 75.75.+a, 75.20.−g, 81.15.Cd

I. INTRODUCTION

The phenomenon of exchange anisotropy or bias (EB) is typically associated with a shift of the hysteresis loop (exchange-bias field, H_E) measured after field-cooling a ferromagnetic (FM)-antiferromagnetic (AFM) interface through the Néel temperature T_N of the AFM component.[1] Other manifestations include an enhanced coercivity and a unidirectional component in torque measurements.[2] This effect has been studied extensively in the last decade due to its application in spin-valves for magnetic reading heads and in random access magnetic storage units, but also because of its fundamental interest, since a number of microscopic models are still a matter of controversy.[3] The simplest material employed to study the EB effect consists of a nanoscale layer or particle of a FM metal, such as Co, which is allowed to passivate in an oxygen atmosphere (CoO is AFM) after its synthesis. Co-CoO bilayers[4–6] and core-shell nanoparticles (NPs)[7–10] are still, in spite of the complex spin structure of CoO, the archetypal systems for exchange-bias studies, given the good growth properties of Co, the convenient (i.e., near room temperature) T_N of CoO (293 K), and the large H_E exhibited by these materials. In addition to the synthesis of such bilayer and NP (Co-CoO) systems, a further approach has been the embedding of core-shell Co-CoO NPs in different types of matrices, recently employed to study the possible stabilization of the FM cores due to the anisotropy contribution from the FM-AFM interface exchange coupling.[11,12]

In this paper the synthesis method of composite bulk film growth in a single step by sputtering Co in an oxygen atmosphere has been employed to prepare exchange-biased Co-CoO material. In contrast to previous work, which has employed this fabrication method to study the structural and magnetic properties of films prepared *as a function of oxygen pressure*,[13–15] in the present work films prepared *as a function of the sputtering power* are investigated. The main result to be presented is that of a minimum occurring in both field-cooled (FC) and zero-field-cooled (ZFC) magnetization curves for films (composites) prepared in a certain sputtering power range. A phenomenological model to explain this feature is proposed, which is supported by results on the effect of sample annealing and x-ray diffraction analysis. The paper begins with the presentation of the resistivity, exchange-bias, and coercivity field of the composites as a function of sputtering power and temperature.

II. EXPERIMENT

The films, several microns thick, were grown on water-cooled glass substrates by magnetron rf sputtering. A high purity Co target was sputtered in an oxygen atmosphere. The argon pressure in the chamber was $p_{Ar}=3\times10^{-3}$ mbar and the oxygen pressure $p_0=3\times10^{-5}$ mbar. Magnetic properties were measured with a commercial vibrating sample magnetometer (VSM) equipped with a cryostat. These properties include hysteresis loops measured at 90 K, and FC and ZFC magnetization curves obtained using a field of 5 kOe (this choice of field will be justified below). All sample cooling was performed from 320 K in a field of 10 kOe, in the case of hysteresis loops, and 5 kOe, in the case of the FC magnetization. Electrical resistivity data were recorded using the four-probe method in a close cycle refrigerator. X-ray diffraction (XRD) was performed using a commercial diffractometer (Philips X'pert), which employed Cu $K\alpha$ radiation. Several samples were submitted to thermal treatments in vacuum, using a furnace adapted to the VSM.

III. RESULTS AND DISCUSSION

Varying the sputtering power between $P=17$ and 75 W produced $Co_x(CoO)_{1-x}$ composites, where x is the volume fraction of the metallic phase, ranging from practically pure fcc CoO (17 W) to nearly pure Co (75 W) with an hcp crystal structure. However, the metallic Co phase (nonoxidized regions) exhibited an fcc structure in samples grown at low rf powers. The increase of the metallic Co fraction with power was followed by x-ray diffraction and saturation magnetization. Resistivity measurements showed the appearance of metallic behavior at $P=24$ W, as shown in Fig. 1. The main

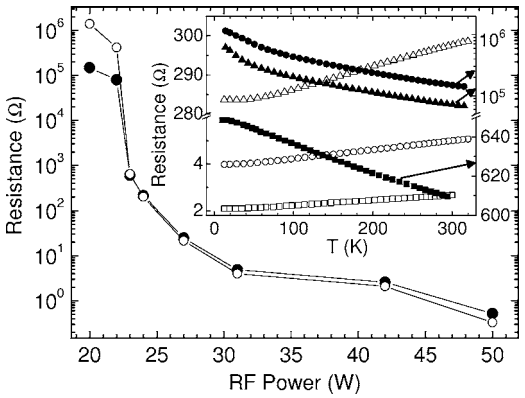

FIG. 1. Sample (electrical) resistance, measured at 30 K (open circles) and 270 K (closed circles), as a function of the rf sputtering power (P) used in sample deposition. The inset shows the temperature dependence of the resistance of three metallic samples (open symbols; $P=24$, 27, and 42 W, from top to bottom; left axis) and three nonmetallic composites (closed symbols; $P=20$, 22, and 23 W, from top to bottom; right axis). Notice the scale breaks in both axes of the inset, as well as the change from linear to logarithmic scale in the right axis.

panel shows the resistance at low ($T=30$ K) and high ($T=270$ K) temperature for each power employed. The intersection of the two curves (change from positive to negative slope in R vs T graphs) takes place at $P=24$ W, a sample with $x=0.53$ (see below). A few representative R vs T curves are plotted in the inset, three corresponding to nonmetallic samples (prepared with powers of 20, 22, and 23 W), and three of metallic character (24, 27, and 42 W). The borderline composite between metallic and nonmetallic character—the sample produced with $P=24$ W—shows a resistivity increase of only 5% from 10 to 300 K.

This first metallic sample of the series ($P=24$ W) exhibits the highest exchange-bias field (hysteresis loop shift), $H_E \approx 2.7$ kOe (measured at 90 K). Five samples of each power batch were measured and have been plotted in Fig. 2, together with the volume concentration of metallic Co as estimated from the saturation magnetization at $T=5$ K. The exchange-bias field is indeed expected to be optimum in the samples with a larger Co-CoO interface density. In this respect, it is worth noting that the samples grown with $P=24$, 27, and 31 W all have a similar metallic Co content ($\sim 50\%$), but the exchange-bias field and the resistivity clearly decrease with increasing power. This behavior can be explained by the larger phase segregation, and therefore lower interface density, resulting from the more energetic deposition associated with higher sputtering powers. These three samples of equal FM Co content also exhibit differences in other magnetic properties, as will be shown later, which justifies the use of the rf sputtering power as the abscissa of the previous figures instead of the concentration x. The rf power dependence of the coercive field essentially mimics that of the exchange-bias field, with values above 4 kOe in the samples prepared using $P=24$ W.

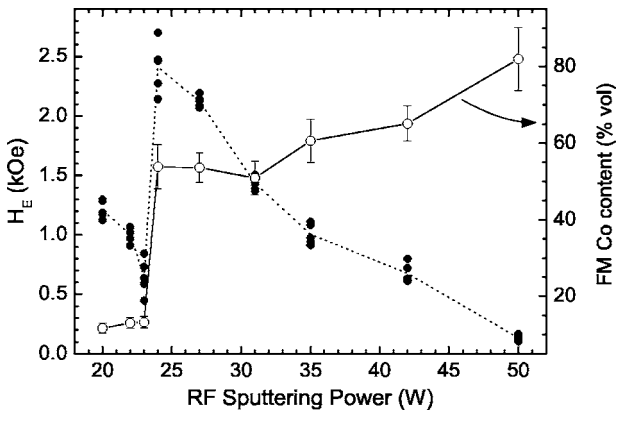

FIG. 2. Sputtering power dependence of the exchange bias field (closed circles; left axis), measured at 90 K, and of the metallic Co content (open circles; right axis). The dispersion in H_E for each power value is due to concentration variations within each sample batch.

The abrupt change in metallic Co content, and thus in exchange bias field, between $P=23$ and 24 W must be remarked. The large dispersion of H_E values in these two batches of samples points to a corresponding dispersion in metallic Co concentration, but it is also enhanced by the sensitivity of the interface density to concentration in the neighborhood of percolation. By sputtering Co in an inert atmosphere, it has been confirmed that the sudden upturn in the metallic Co concentration is not related to the deposition rate of pure Co, which is linear in the studied power range. The overall deposition rate (Co+CoO) does not show any abrupt variation either. The feature can be explained after the work of Hecq *et al.*[16] (whose conclusions are outlined in Ref. 13). For low rf powers, the sputtering rate is lower than the oxidation rate of the Co target, thus mostly cobalt oxides are sputtered. For higher powers, the sputtering rate becomes higher than the oxidation rate, and thereby the sputtered material is mainly Co. The observed abrupt change in concentration reflects the crossover between the two sputtering regimes.

Figure 3 shows the temperature dependence of the exchange-bias and coercive fields for five representative samples: two nonmetallic (20 and 23 W) and three metallic composites (24, 35, and 42 W). The data have been extracted from hysteresis loops measured at 90 K after sample cooling from 320 K in a field of 10 kOe. The exchange-bias blocking temperature, $T_b \approx 275$ K, is close to the bulk CoO Néel temperature in samples belonging to the former group (Co concentrations below $x \approx 0.55$), whereas the loop shift vanishes at $T_b \approx 220$ K in all samples deposited using $P > 24$ W, pointing to a dependency of the blocking temperature on the concentration of the AFM component. Regarding the coercive field, the samples with low x ($P=20$ and 23 W) display a peak at about 275 K. This peak is a well-known feature in exchange-biased systems, either core-shell structured particles or bilayers.[2] It has been explained in terms of a reduction of the anisotropy of the AFM component as its ordering temperature is approached, an effect which allows more spins to be dragged irreversibly by the rotation of the FM moments. We have observed this feature sharply only in nonpercolated composites and very faintly in the borderline sample prepared with 24 W. Interestingly, close inspection of the higher power samples [Fig. 3(b)], however, reveals the

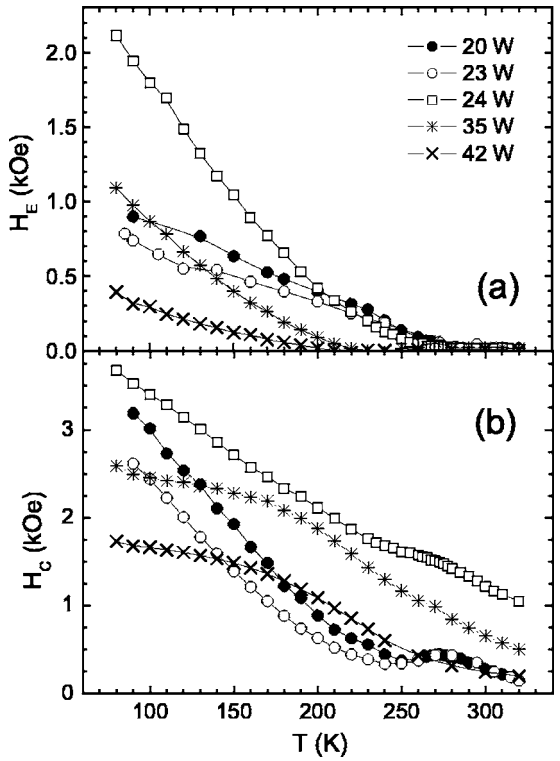

FIG. 3. Temperature dependence of (a) the exchange bias and (b) the coercivity fields for composites grown at different rf powers.

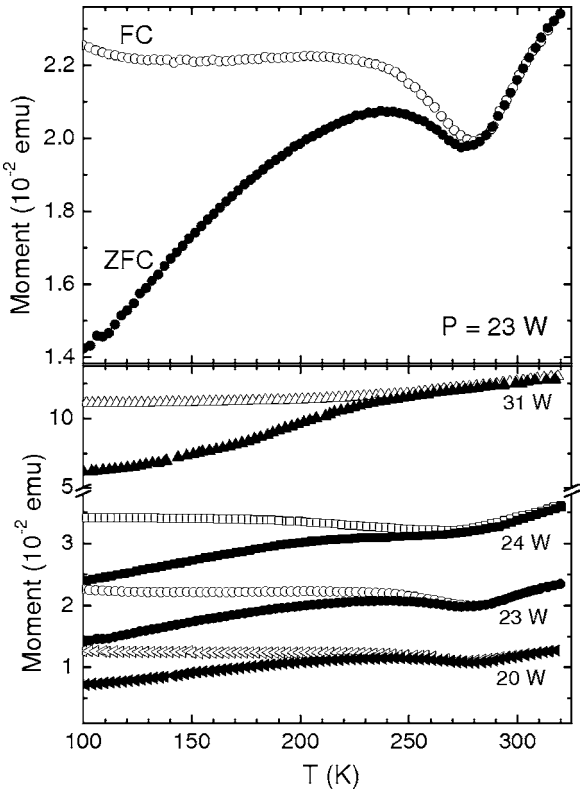

FIG. 4. Field-cooled (empty symbols) and zero-field-cooled (solid symbols) magnetic moment, measured using a field $H=5$ kOe, of four composites grown at different rf powers (P). The upper panel shows, in more detail, the dip exhibited by the $P=23$ W sample.

presence of a hump, rather than a peak, around the onset of the exchange-bias effect. X-ray diffraction indicates that these higher power samples possess smaller CoO grains than the $P \leqslant 24$ W samples, leading to their lower blocking temperature. The broadness of the hump can be explained by a wider CoO grain size distribution.[2]

The temperature dependence of the FC and ZFC magnetization provides information on the Co regions, since these regions determine the magnetic signal. The FC and ZFC magnetization curves measured in three representative samples ($P=23$, 24, and 31 W), using $H=5$ kOe, are plotted in Fig. 4. The strong FC-ZFC irreversibility (present in all samples, but diminishing with increasing power) indicates that the size of a significant fraction of the metallic Co regions lies in the nanoscale, their magnetic moments blocking at random directions (along the effective anisotropy axis of each region) when the sample is cooled in zero field. A rarer feature appears in the magnetization of samples deposited with $P<27$ W: a pronounced dip, in both the FC and ZFC curves, at $T \approx 275$ K, precisely the exchange-bias blocking temperature of those samples (as seen in Fig. 3). The minimum is more pronounced in the nonmetallic samples (the upper panel shows in more detail the magnetization of the sample prepared with 23 W), and is smeared-out beyond the borderline sample ($P=24$ W) until fully disappearing for $P=31$ W. A similar dip was also observed with ac susceptibility (not shown). This feature, the absence of which may be taken as a signature of metallic percolation in this type of composite, is most probably due to the loss of magnetic stability in isolated Co NPs (surrounded by CoO), as the effective contribution of the exchange-bias to the magnetic anisotropy vanishes above the AFM ordering temperature of the matrix. The magnetic stabilization of NPs, i.e., the increase of their superparamagnetic blocking temperature, using exchange anisotropy has indeed been demonstrated in granular materials with Co-CoO core-shell NPs embedded in either a CoO matrix[11] and, more recently, in a nonmagnetic matrix (Ag).[12] It has also been demonstrated in colloidal Co NPs allowed to oxidize to different extents.[9] These small FM NPs separated from one another by AFM material would constitute a significant fraction of the metallic Co phase only in nonpercolated samples, thus explaining our observations. The dip was best observed measuring with a field of $H \approx 5$ kOe, as at this field the loss of magnetization due to the thermal destabilization of the small particles relative to the total magnetization is maximized, i.e., the depth of the dip is maximized. This field was determined experimentally by subtracting the hysteresis loop measured at the dip ($T=275$ K) from the loop measured at the beginning of the dip ($T=275$ K), the difference being largest for $H \approx 5$ kOe. The magnetization at this field is roughly half the saturation value.

The results presented so far suggest a simple structural model whereby metallic Co is found in three regimes, which are defined according to their associated magnetic behavior.

(i) Isolated NPs, so small that upon heating from low temperatures they become unstable when the AFM order of the CoO matrix (and thus the exchange anisotropy) is lost, as explained above.

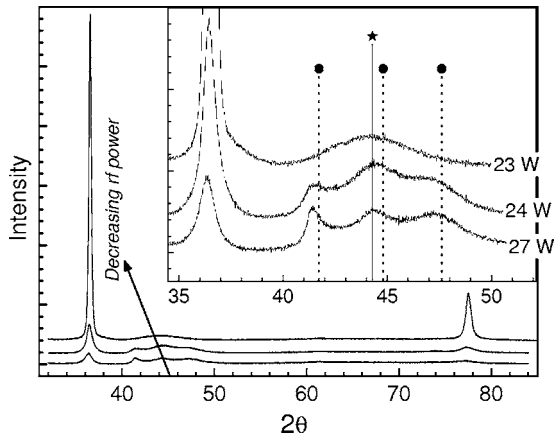

FIG. 5. Specular ($\theta/2\theta$) x-ray diffraction patterns of the composites prepared with sputtering powers $P=23$, 24, and 27 W. The inset is an enlarged 2θ region where the progressive change of the Co structure from fcc to hcp with increasing rf power can be observed. The reflection positions marked are for bulk Co: the (111) fcc (star symbol) and, for increasing 2θ, the (100), (002), and (101) hcp (solid circles).

(ii) Larger particles, large enough to be stable over the entire (accessible) temperature range, but still highly anisotropic and thereby accounting for most of the observed FC-ZFC irreversibility. The superparamagnetic blocking temperature of these particles is beyond the highest measured temperature (320 K), as is apparent from the still increasing magnetization at 320 K, which implies that the onset of the FC-ZFC irreversibility would have taken place at higher temperatures had the sample cooling been initiated at higher temperatures. The magnetization dips in both curves result from the superposition of the magnetization contribution of these large particles with that of the fine particles described in (i).

(iii) Yet larger (probably multidomain) regions, which give the FM background apparent in Fig. 4, since they can be easily magnetized and do not yield any thermally hysteretic magnetization.

Our observation is that the relative fraction of these forms, as reflected by their corresponding fingerprints in the overall magnetization (dip at $T \approx T_b$, FC-ZFC irreversibility, and FM background, respectively) shifts in the indicated order [(i)$\rightarrow$(iii)] as the rf sputtering power, and thus the Co concentration and the size of the Co regions, increases, as would be expected.

The simple microstructural model given above is supported by XRD analysis of the samples. Figure 5 shows the specular ($\theta/2\theta$) patterns registered in three samples spanning the crossover region ($P=23$, 24, and 27 W). For the $P=23$ W sample, in addition to two intense reflections corresponding to well textured (along $\langle 111 \rangle$) fcc CoO, there is a broad peak centered very close to the (111) position of bulk[17] fcc Co. Attributing the Lorentzian-like profile of this broad peak to (Scherrer) grain size effects alone gives an estimate of the Co fcc grain size (D) of 2.5 nm. Given that the fcc structure is typically found in Co NPs,[9] including particles embedded in various matrices,[18–20] in contrast to the majority hcp structure present in bulk Co, it is logical to identify a fraction of these fine Co grains as the physically separated NPs described in point (i) of our model (their very small size is in good agreement with the observed magnetic destabilization when the exchange bias effect is lost at $T > T_b$), and the larger particles described in point (ii) to be multigrain particles composed of the remaining fraction of these grains.

For the $P=24$ and 27 W samples, which show less intense CoO peaks (Fig. 5), three reflections at positions very close to those of the (100), (002), and (101)—in order of increasing 2θ—positions of bulk[21] hcp Co are observed (inset). This establishes the presence of hcp Co grains in the samples. As the fcc Co (111) position is very close to that of the hcp (002), it is not possible to determine, from a simple visual inspection of the XRD data, whether a Co fcc phase is also present in both composites. Since analysis of the $P=23$ W identifies 2.5 nm fcc Co NPs to be the particles described in point (i), which give rise to the dip in the magnetization, and in the $P=24$ and 27 W samples the dip is still observed—but increasingly smeared out with increasing sputtering power (Fig. 4)—it is reasonable to expect that a fraction of fcc Co NPs are still present in these two composites. To determine whether this is the case, we have analyzed the XRD patterns from these two composites using the Rietveld method. Former structural studies of such materials[13–15] have, for certain preparation conditions, observed similar diffraction patterns in the region of the three hcp reflections as those for the $P=24$ and 27 W samples. However, of these studies, only when TEM was used[14] for complementary structural characterization was the presence of fcc Co (in addition to hcp) concluded.

Rietveld refinements were performed with the program RIETICA,[22] using a Voigt reflection profile for each phase. The (dominant) Lorentzian component to each profile was attributed to grain size alone (and the parameters of the less significant Gaussian part were fixed to values typical of the instrument resolution function). Figure 6 shows the refinement of the XRD pattern from the $P=24$ W sample to three phases: hcp Co (A), fcc Co (B), and fcc CoO (C). Attempting to fit to just two phases—hcp Co and fcc CoO—produced, in the region of the three close reflections, a fit inferior to that in Fig. 6. The lattice parameter and grain size (D) for the Co fcc phase were held fixed at the values determined from the analysis of the $P=23$ W sample. Other grain sizes are estimated to be 5.7 nm (hcp Co) and 13.1 nm (fcc CoO). Allowing the grain size of the Co fcc phase to vary produced a negligible change with respect to the value determined for the $P=23$ W sample. All three phases (Fig. 6) are found to exhibit preferred orientation (PO), the PO axes being: $\langle 100 \rangle$ (A), $\langle 111 \rangle$ (B), and $\langle 111 \rangle$ (C); and the PO parameters, G_1 (from a Dollase model[23]), are 0.53 (A), 0.30 (B), and 0.281 (C). The (Rietveld) scale factors for the Co hcp and Co fcc phases are consistent with the former phase being the most abundant of the two.

The occurrence of both Co phases, hcp and fcc, in the 24 W sample, with the former phase being the more abundant and possessing the larger grain size of the two phases, is consistent with the model drawn from the magnetic behavior. In this sample, the hcp grains would form both some of the large particles [described in point (ii)] and the large regions [point (iii)], and the finer fcc (Co) grains would (as in the

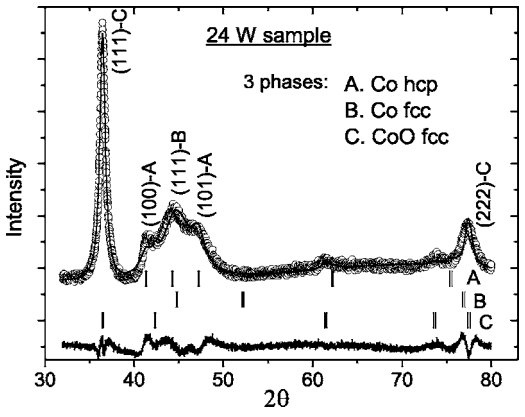

FIG. 6. Rietveld fit of the x-ray diffraction pattern of the composite grown with sputtering power $P=24$ W. The fit is to three phases: (A) hcp Co, (B) fcc Co, and (C) fcc CoO. The difference curve (data-fit) is shown, along with the reflection bars for each phase (these are doublets at high 2θ due to the (Cu) $K\alpha_1$ and $K\alpha_2$ components of the incident x-ray beam). The reliability factors, R_p and R_{wp}, of the fit are 4.4% and 5.6%, respectively. The main reflection contributing to each (observable) peak in the pattern is labeled.

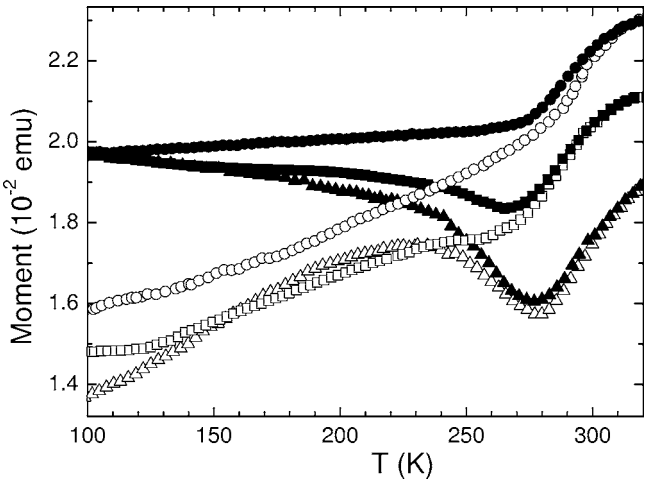

FIG. 7. Field-cooled (open symbols) and zero-field-cooled (closed symbols) magnetic moment, measured with a field of $H=5$ kOe, of the sample grown with $P=23$ W: as-deposited (triangles), after annealing up to 240 °C (squares), and after annealing up to 290 °C (circles).

23 W sample) form the ultrafine NPs [point (i)] and the remaining large particles [point (ii)]. The large particles [point (ii)] in the 24 W sample are thus considered to be formed by both the hcp and fcc Co grains.

Moving to the $P=27$ W sample, Rietveld analysis determines, from a reduction of the scale factor for the Co fcc phase relative to that of the Co hcp, that the hcp phase is yet more abundant than in the 24 W sample. This is consistent with the smearing-out of the minimum in the magnetization curves (Fig. 4) above the sputtering power of 24 W, i.e., a reduction in the abundance of Co fcc grains (from 24 to 27 W) would be concomitant with a reduction in the number of isolated NPs [of the type described in point (i)]. At still higher rf powers, the Co hcp peaks dominate the XRD pattern, and, thus the magnetic behavior is entirely associated to Co hcp grains that would form large particles [point (ii)] and large regions [point (iii)].

Finally, in order to confirm the origin of the dip in the magnetization of low x samples, the composite obtained with $P=23$ W was subjected to successive thermal treatments (each of 20 min duration) at increasingly higher annealing temperatures, and the FC and ZFC magnetization recorded after each annealing. The resulting data, displayed in Fig. 7, show that thermal treatments at temperatures as low as 240 °C are enough to affect the magnetization dip, which disappears after annealing up to 290 °C. This is due to the thermally induced progress of segregation of the Co and CoO phases, which involves the growth, through coalescence, of the (fcc) Co particles. This growth is indicated by a narrowing of the Co fcc (111) peak in the XRD pattern (not shown). The magnetization dip is thus clearly related to the presence of a fraction of sufficiently small Co particles in the sample.

The reduction of interface density caused by the segregation of the FM and AFM components upon annealing is sensitively detected by a large drop in the exchange bias field, as shown in Fig. 8. Moreover, the disappearance of the magnetization dip is accompanied by that of the peak in the temperature dependence of the coercivity (see Fig. 8, lower panel), suggesting that the aforementioned dragging of AFM spins at the interfaces takes place more effectively during the magnetization reversal of fine NPs, as compared to the mag-

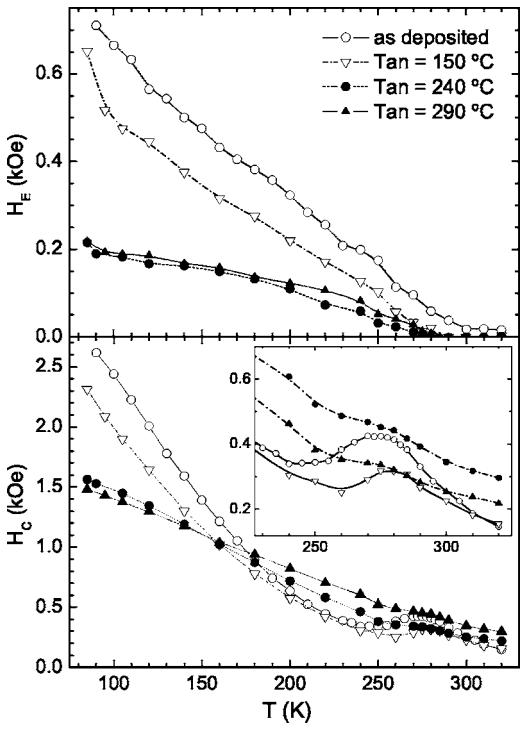

FIG. 8. Temperature dependence of the exchange bias (upper panel) and coercivity (lower panel) fields of the sample grown with $P=23$ W: as-deposited (open circles), after annealing up to 150 °C (open triangles), up to 240 °C (closed circles), and up to 290 °C (closed triangles). The inset in the lower panel focuses on the peak region.

netization of larger particles, where the rotation of the magnetization might not be as coherent.

IV. CONCLUSIONS

In summary, a series of Co-CoO composites have been fabricated by the simple method of reactive sputtering of Co, and their magnetic properties as a function of sputtering power (and thus composition) have been related to their microstructure. In particular, a remarkable dip in the temperature dependence of the magnetization has been shown to stem from the destabilization of fine Co NPs as the CoO matrix surrounding them loses its AFM order. This phenomenon may be observed in future magnetization studies of Co-CoO films prepared under different reactive sputtering conditions (e.g., by varying oxygen pressure, as in Refs. 13–15), where such fine Co NPs are present.

ACKNOWLEDGMENTS

This work was supported financially by the Spanish CICYT (MAT 2002-03490) and the Ministerio de Educación y Ciencia (P. S. Normile, SB 2004-0071). We thank M. Rivera and E. Prado for their expert technical support in sample preparation.

[1] W. H. Meiklejohn and C. P. Bean, Phys. Rev. **102**, 1413 (1956); **105**, 904 (1957).
[2] J. Nogués and I. K. Schuller, J. Magn. Magn. Mater. **192**, 203 (1999).
[3] M. Kiwi, J. Magn. Magn. Mater. **234**, 584 (2001).
[4] S. Brems, D. Buntinx, K. Temst, C. Van Haesendonck, F. Radu, and H. Zabel, Phys. Rev. Lett. **95**, 157202 (2005).
[5] C. Binek, X. He, and S. Polisetty, Phys. Rev. B **72**, 054408 (2005).
[6] F. Radu, M. Etzkorn, R. Siebrecht, T. Schmitte, K. Westerholt, and H. Zabel, Phys. Rev. B **67**, 134409 (2003).
[7] D. L. Peng, K. Sumiyama, T. Hihara, S. Yamamuro, and T. J. Konno, Phys. Rev. B **61**, 3103 (2000).
[8] S. Gandopadhyay, G. C. Hadjipanayis, C. M. Sorensen, and K. J. Klabunde, J. Appl. Phys. **73**, 6965 (1993).
[9] J. B. Tracy, D. N. Weiss, D. P. Dinega, and M. G. Bawendi, Phys. Rev. B **72**, 064404 (2005).
[10] J. Nogués, J. Sort, V. Langlais, V. Skumryev, S. Suriñach, J. S. Muñoz, and M. D. Baró, Phys. Rep. **422**, 65 (2005).
[11] V. Skumryev, S. Stoyanov, Y. Zhang, G. Hadjipanayis, D. Givord, and J. Nogués, Nature (London) **423**, 850 (2003).
[12] J. M. Riveiro, J. A. De Toro, J. P. Andrés, J. A. González, T. Muñoz, and J. P. Goff, Appl. Phys. Lett. **86**, 172503 (2005).
[13] J. Y. Yi, C. L. Platt, M. L. Rudee, A. E. Berkowitz, and T. L. Cheeks, J. Appl. Phys. **79**, 5072 (1996).
[14] J. B. Yi, J. Ding, B. H. Liu, Z. L. Dong, T. White, and Y. Liu, J. Magn. Magn. Mater. **285**, 224 (2005).
[15] T. Yamauchi and K. Shiiki, Jpn. J. Appl. Phys., Part 1 **41**, 5982 (2002).
[16] M. Hecq, A. Hecqet, and J. Van Cakenberghe, Thin Solid Films **42**, 97 (1977).
[17] F. Aldinger and S. Jönsson, Z. Metallkd. **68**, 362 (1977).
[18] R. H. Kodama and A. S. Edelstein, J. Appl. Phys. **85**, 4316 (1999).
[19] J. C. Cezar, H. C. N. Tolentino, and M. Knobel, Phys. Rev. B **68**, 054404 (2003).
[20] J. A. De Toro, J. P. Andrés, J. A. González, J. P. Goff, A. J. Barbero, and J. M. Riveiro, Phys. Rev. B **70**, 224412 (2004).
[21] K. H. J. Buschow, P. G. Van Engen, and R. Jongebreur, J. Magn. Magn. Mater. **38**, 1 (1983).
[22] B. Hunter, Newsletter 20, IUCR (1998), available at: http://www.iucr.org/iucr-top/comm/cpd/Newsletters/no20summer1998/art15/art15. htm.
[23] W. A. Dollase, J. Appl. Crystallogr. **19**, 267 (1986).